doi:10.3772/j.issn.1006-6748.2020.03.006

Image texture smoothing method by a novel L_0 -norm optimization model①

Nie Dongdong (聂栋栋)*, Ge Xindi②*, Zhang Tianlai**
(*College of Sciences, Yanshan University, Qinhuangdao 066004, P. R. China)
(**Bank of Xingtai, Xingtai 054001, P. R. China)

Abstract

Texture smoothing is a fundamental tool in various applications. In this work, a new image texture smoothing method is proposed by defining a novel objective function, which is optimized by L_0-norm minimization and a modified relative total variation measure. In addition, the gradient constraint is adopted in objective function to eliminate the staircase effect, which can preserve the structure edges of small gradients. The experimental results show that compared with the state-of-the-art methods, especially the L_0 gradient minimization method and the relative total variation method, the proposed method achieves better results in image texture smoothing and significant structure preserving.

Key words: texture smoothing, structure preserving, L_0-norm minimization, relative total variation

0 Introduction

The key to texture smoothing[1,2] is to remove small textures while preserving the significant edges and structures in the images. Texture smoothing is used in many fields, such as image segmentation[3,4], edge detection[5,6], object recognition[7,8] and image enhancement[9-11]. Although several proposed variation models are very effective for removing image noise, they cannot distinguish image structures and textures effectively. In Ref. [12], an L_0-norm minimization algorithm is proposed to restrain the number of non-zero image gradients and produce a global sparse solution, which can preserve the image significance structure and remove detail textures and noises effectively. The advantage of the L_0minimization is that it can smooth texture and preserve edges better than others, such as the weighted least square (WLS)[13], and bilateral filter (BLF)[14]. Shen et al.[15] extended the L_0 objective function by adopting L_1-norm instead of L_2-norm in the data fidelity term and achieved some promising results. Cheng et al.[16] presented a novel approximation algorithm for L_0 gradient minimization in a fused coordinate descent framework. Unfortunately, since these methods highly depend on the magnitude of image gradients, and image gradients haven't enough structure extraction ability, the methods mentioned above cannot remove high contrast texture details effectively.

Xu et al.[17] defined a new relative total variation (RTV), in which textures and main structures show completely different properties, and presented an optimization framework based on RTV regularization term for structure-texture decomposition. Since then, many scholars have made further research on RTV to improve the discrimination between textures and structures. Ref. [18] defined a modified relative total variation (mRTV) to make it more suitable in L_0-norm minimization by proposing a new function. mRTV is small in texture regions and large along structure edges. Liu et al.[19] made further extension of RTV and proposed a general relative total variation (GRTV) model by expanding the norm of windowed total variation (WTV) in RTV from 0 to [0,1].

This work presents a novel L_0-norm optimization model, which combines the data fidelity term, a new gradient fidelity term and a regularization term based on the L_0-norm of mRTV. Due to the non-convex and non-linear property of the optimization model, it is a challenge to obtain the solution directly. Subsequently, an efficient approximate solution is also given. It can be found that the difference between textures and main structures becomes larger with the increase of the parameter α in the proposed model. The most important

① Supported by the National Natural Science Foundation of China Youth Fund (No. 61807029) and Natural Science Foundation of Hebei Province (No. F2019203427).

② To whom correspondence should be addressed. E-mail: gexindi@126.com

Received on Sep. 16, 2019

thing is that the results are not only sufficiently similar to the original images but also have clear edges and suppressed textures.

This paper includes 4 sections. Section 1 briefly reviews the definition of mRTV measure and the L_0 gradient minimization method. Section 2 presents the optimization framework with a new gradient consistency constraint and mRTV sparse constraint. Section 3 discusses the parameters of the proposed optimization model and gives some comparison experiments. The conclusion is in Section 4.

1 Related background

Here the notations used in this work are giving in Table 1.

Table 1 Explanation of notations

Notation	Explanation	Notation	Explanation
$\Re$	Modified relative total variation	I/S	Input/Output image
φ	Windowed total variation	∇S	Gradient of S
ϕ	Windowed inherent variation	λ	Smoothing parameter
σ	The spatial scale of texture	β	Similarity parameter
α	Accentuate structures from textures	δ,ρ	Auxiliary variables
$w_{p,q}$	Gaussian weighting function	η,γ	Auxiliary variables

1.1 Modified RTV measure

Based on the relative total variation, Ref. [18] proposed modified RTV measure, which is expressed as

$$\Re(p) = \Re_x(p) + \Re_y(p) \tag{1}$$

where

$$\Re_d(p) = s\varphi_d(p)\phi_d(p)^{\alpha} \tag{2}$$

$$\varphi_d(p) = \sum_{q\in\Omega_p} \omega_{p,q} \cdot |\partial_d I_q| \tag{3}$$

$$\phi_d(p) = \sum_{q\in\Omega_p} |\omega_{p,q} \cdot \partial_d I_q| \tag{4}$$

$$\omega_{p,q} = \exp\left(-\frac{|p-q|^2}{2\sigma^2}\right) \tag{5}$$

here s is the normalization factor, I represents the input image, Ω_p is the set of pixels in the local neighborhood centered at p point, and $\partial_d I$ denote the partial derivatives of I along the x and y directions respectively, $d \in \{x, y\}$ represents the direction to compute the partial derivatives, $|\cdot|$ indicates the absolute value of a number, $\omega_{p,q}$ is a Gaussian weighting function. α is used to enhance the discrimination between structures and textures.

Compared with RTV, the modified RTV adopts an exponent parameter α to accentuate the image structures, and uses multiplication instead of division to make the mRTV values bigger along edges and smaller for textures, which makes it more suitable to L_0-norm minimization.

1.2 L_0 gradient minimization

L_0-norm directly measures the sparsity of a vector, so L_0-norm minimization is usually used to obtain a sparse solution. Many algorithms adopt it for texture details smoothing or significant edge structures extracting. However, due to the non-convexity of the L_0-norm, it is difficult to be minimized directly. In Ref. [12], for the task of image texture smoothing, a split method was applied to solve the L_0-norm minimization problem, which achieved good results.

Assuming that I represents the input image, S is the output image. The vector $(\partial_x S_p, \partial_y S_p)^{\mathrm{T}}$ for each pixel p is calculated as the partial derivatives of S along the x and y directions respectively. Then the L_0-norm measures of the image S gradients is the number of non-zero gradients, which can be defined by

$$C(S) = \#\{p \mid |\partial_x S_p| + |\partial_y S_p| \neq 0\} \tag{6}$$

According to the definition in Eq. (6), the model of image texture smoothing method based on the gradient L_0-norm minimization can be written by

$$\min_S \{\sum_p (S_p - I_p)^2 + \lambda \cdot C(S)\} \tag{7}$$

The data term $(S_p - I_p)^2$ is to make the output image similar to the input image. The second term $\lambda \cdot C(S)$ is a regular term, also known as a smooth term to ensure the gradient sparseness of the output image. λ is a non-negative parameter controlling the significance of $C(S)$.

2 Proposed method

The framework of the proposed method is shown in Fig. 1. Different from above 2 methods, for an input image I, the output smoothed image S is calculated by solving the following objective function.

$$\min_S \{\|S - I\|_2^2 + \|\nabla S - \nabla I\|_2^2 + \lambda \cdot |\Re|_0\} \tag{8}$$

where ∇ is the gradient operator, the second term is the gradient fidelity term which ensures that the gradient of the output image S is similar to that of input image I, $\lambda \cdot |\Re|_0$ indicates the L_0-norm of the mRTV measure of the output image S, which directly measures the sparseness of mRTV and ensures the smoothness of the image S.

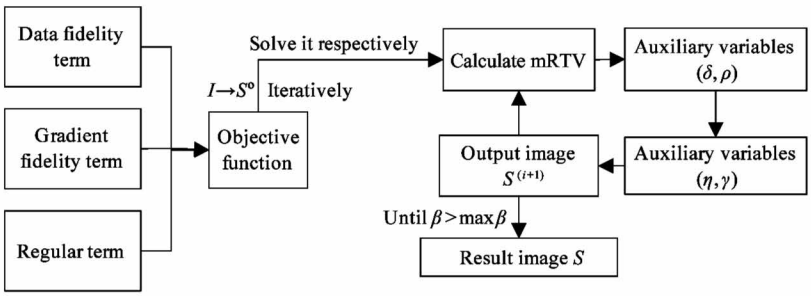

Fig. 1 Framework of this proposed method

Due to the non-convexity of the L_0-norm and the non-linearity of mRTV, it is hard to solve Eq. (8) by using traditional gradient decent method directly. Inspired by the methods of Refs[12] and [18], an alternating optimization strategy is adopted to solve it iteratively.

In particular, considering the non-negativity of $\Re_x$ and $\Re_y$, two non-negative auxiliary variables δ and ρ respectively corresponding to $\Re_x$ and $\Re_y$ are introduced, then the Eq. (8) is equivalent to the following function:

$$\min_{S,\delta,\rho} \| S - I \|_2^2 + \| \nabla S - \nabla I \|_2^2 + \beta \cdot (\| \Re_x - \delta \|_2^2 + \| \Re_y - \rho \|_2^2) + \lambda \cdot | \delta + \rho |_0 \tag{9}$$

The first 2 terms are the data term and the gradient fidelity term, the third term controls the smoothness of the output image S. β is the adaptive parameter for controlling the similarity between (δ, ρ) and $(\Re_x, \Re_y)$. The fourth term controls the sparseness of the sum of non-negative auxiliary variables δ and ρ.

Define a binary function:

$$H(\delta_p, \rho_p) = \begin{cases} 1 & \delta_p + \rho_p \neq 0 \\ 0 & \text{others} \end{cases} \tag{10}$$

The Eq. (9) can be expressed as

$$\min_{S,\delta,\rho} \sum_p ((S_p - I_p)^2 + (\nabla S_p - \nabla I_p)^2) + \sum_p (\beta \cdot ((\Re_x(p) - \delta_p)^2 + (\Re_y(p) - \rho_p)^2) + \lambda \cdot H(\delta_p, \rho_p)) \tag{11}$$

For the sake of simplicity, the nonlinear objective function Eq. (11) is transformed into 2 separate problems and solve it iteratively.

2.1 Solving (δ, ρ)

Fixing the output image S, then the Eq. (11) can be represented by

$$\min_{\delta,\rho} \sum_p ((\Re_x(p) - \delta_p)^2 + (\Re_y(p) - \rho_p)^2 + \frac{\lambda}{\beta} \cdot H(\delta_p, \rho_p)) \tag{12}$$

Let

$$B_p = (\Re_x(p) - \delta_p)^2 + (\Re_y(p) - \rho_p)^2 + \frac{\lambda}{\beta} \cdot H(\delta_p, \rho_p) \tag{13}$$

If $(\Re_x(p))^2 + (\Re_y(p))^2 \leqslant \frac{\lambda}{\beta}$

i) When $\delta_p + \rho_p \neq 0$ and $H(\delta_p, \rho_p) = 1$

$$B_p((\delta_p, \rho_p) \neq (0,0)) = (\Re_x(p) - \delta_p)^2 + (\Re_y(p) - \rho_p)^2 + \frac{\lambda}{\beta} \geqslant \frac{\lambda}{\beta} \geqslant (\Re_x(p))^2 + (R_y(p))^2 \tag{14}$$

ii) When $\delta_p + \rho_p = 0$, that is $(\delta_p, \rho_p) = (0, 0)$, and $H(\delta_p, \rho_p) = 0$

$$B_p((\delta_p, \rho_p) = (0, 0)) = (\Re_x(p))^2 + (\Re_y(p))^2 \leqslant \frac{\lambda}{\beta} \tag{15}$$

So the minimum energy $B_p = (\Re_x(p))^2 + (\Re_y(p))^2$ is acquired when $(\delta_p, \rho_p) = (0, 0)$.

If $(\Re_x(p))^2 + (\Re_y(p))^2 > \frac{\lambda}{\beta}$

i) When $\delta_p + \rho_p \neq 0$ and $H(\delta_p, \rho_p) = 1$

$$B_p((\delta_p, \rho_p) \neq (0, 0)) = (\Re_x(p) - \delta_p)^2 + (\Re_y(p) - \rho_p)^2 + \frac{\lambda}{\beta} \geqslant \frac{\lambda}{\beta} \tag{16}$$

ii) When $\delta_p + \rho_p = 0$ and $H(\delta_p, \rho_p) = 0$

$$B_p((\delta_p, \rho_p) = (0, 0)) = (\Re_x(p))^2 + (\Re_y(p))^2 > \frac{\lambda}{\beta} \tag{17}$$

So the minimum energy $B_p = \frac{\lambda}{\beta}$ is acquired when

$(\delta_p, \rho_p) = (R_x(p), \Re_y(p))$.

In summary, Eq. (12) has solution:

$$(\delta_p, \rho_p) = \begin{cases} (0, 0) & \Re_x(p)^2 + \Re_y(p)^2 \leqslant \dfrac{\lambda}{\beta} \\ (\Re_x(p), \Re_y(p)) & \text{others} \end{cases} \tag{18}$$

2.2 Solving S

Fixing δ and ρ, the S-estimation problem corresponds to minimizing:

$$\min_S \sum_p ((S_p - I_p)^2 + (\nabla S_p - \nabla I_p)^2 + \beta \cdot ((R_x(p) - \delta_p)^2 + (R_y(p) - \rho_p)^2)) \tag{19}$$

Due to the non-linearity of $\Re_x$ and $\Re_y$, the above objective equation is still difficult to be solved. Eq. (19) is decomposed into a relatively simple problem and solve it iteratively.

In order to make the formula look more concise, let $\chi_d(p) = s\phi_d(p)^\alpha$, then $\Re_d(p) = \chi_d(p)\varphi_d(p)$.

Take $\Re_x$ as an example, its non-linearity can be eliminated by approximately expanding the $(\Re_x(p) - \delta_p)^2$ term in Eq. (19) as

$$\begin{aligned} (\Re_x(p) - \delta_p)^2 &= (\chi_x(p) \cdot \sum_{q \in \Omega(p)} \omega_{p,q} \mid \partial_x S_q \mid - \delta_p)^2 \\ &= (\chi_x(p) \cdot \omega_{p,p} \mid \partial_x S_p \mid + \chi_x(p) \cdot \sum_{q \in \Omega(p)}^{q \neq p} \omega_{p,q} \mid \partial_x S_q \mid - \delta_p)^2 \\ &\approx (\hat{\chi}_x(p) \cdot \omega_{p,p} \mid \partial_x S_p \mid + \hat{\chi}_x(p) \cdot \sum_{q \in \Omega(p)}^{q \neq p} \omega_{p,q} \mid \partial_x \hat{S}_q \mid - \delta_p)^2 \\ &= (k_{xp} \mid \partial_x S_p \mid + b_{xp})^2 \end{aligned} \tag{20}$$

$$k_{xp} = \hat{\chi}_x(p) \cdot \omega_{p,q} \tag{21}$$

$$b_{xp} = \hat{\chi}_x(p) \cdot \sum_{q \in \Omega(p)}^{q \neq p} \omega_{p,q} \mid \partial_x \hat{S}_q \mid - \delta_p \tag{22}$$

where $\hat{\chi}$ and $\hat{S}$ indicate the results of the last iteration, and k_{xp}, b_{xp} are 2 constants. Eq. (20) has minimum when $\mid \partial_x S_q \mid = -\dfrac{b_{xp}}{k_{xp}}$.

$$\begin{aligned} \mid \partial_x S_q \mid &= -\frac{b_{xp}}{k_{xp}} = -\frac{\hat{\chi}_x(p) \cdot \sum_{q \in \Omega(p)}^{q \neq p} \omega_{p,q} \mid \partial_x \hat{S}_q \mid - \delta_p}{\hat{\chi}_x(p) \cdot \omega_{p,p}} \\ &= \begin{cases} -\sum_{q \in \Omega(p)}^{q \neq p} \dfrac{\omega_{p,q} \mid \partial_x \hat{S}_q \mid}{\omega_{p,p}} & \delta_p = 0 \\ \mid \partial_x \hat{S}_q \mid & \delta_p = \hat{R}_x(p) \end{cases} \end{aligned} \tag{23}$$

Noticed that $-\sum_{q \in \Omega(p)}^{q \neq p} \dfrac{\omega_{p,q} \mid \partial_x \hat{S}_q \mid}{\omega_{p,p}}$ is always negative, which is impossible in reality unless $\mid \partial_x \hat{S}_q \mid = 0$. Therefore, the Eq. (23) achieves a minimum value under the following conditions:

$$\partial_x S_p = \begin{cases} 0 & \delta_p = 0 \\ \partial_x \hat{S}_p & \delta_p = \hat{R}_x(p) \end{cases} \tag{24}$$

Similarly, the above derivation can be also applied to eliminate the non-linearity of $R_y(p)$.

As a result, the Eq. (19) can be transformed into the following quadratic minimization problem:

$$\min_S \sum_p ((S_p - I_p)^2 + (\nabla S_p - \nabla I_p)^2 + \beta \cdot ((\partial_x S_p - \eta_p)^2 + (\partial_y S_p - \gamma_p)^2)) \tag{25}$$

Here η, γ only depends on auxiliary variables δ, ρ

$$(\eta_p, \gamma_p) = \begin{cases} (0,0) & (\delta_p, \rho_p) = (0,0) \\ (\partial_x S_p, \partial_y S_p) & (\delta_p, \rho_p) = (\Re_x(p), \Re_y(p)) \end{cases} \tag{26}$$

Therefore, it can be learned that the solution of Eq. (25) converges to the solution of Eq. (19). Eq. (25) is quadratic, and thus it can be solved easily.

By diagonalizing the partial derivative operators and the accelerating fast Fourier transform (FFT), the solution of Eq. (25) in each iteration is

$$S = F^{-1}\left(\frac{F(I) + L + \beta \cdot M}{1 + (1 + \beta) \cdot N}\right) \tag{27}$$

where

$$L = N \cdot F(I) \tag{28}$$

$$M = F(\partial_x)^* \cdot F(\eta) + F(\partial_y)^* \cdot F(\gamma) \tag{29}$$

$$N = F(\partial_x)^* \cdot F(\partial_x) + F(\partial_y)^* \cdot F(\partial_y) \tag{30}$$

here F is the FFT operator, F^* denotes the conjugate of F. The multiplication and division are all component-wise operators.

Algorithm 1 sketches the procedure of the proposed method. Fig. 2 exhibits the results of different iterations. Here, it only needs 3 iterations to get a texture smoothing results. It is shown that the approximate solution given in the above deduction has a very fast convergence speed and the objective function constructed in this study is effective to texture smoothing and edge preserving.

Algorithm1: The proposed image texture smoothing method

1 **Input**: image I, gradient weight α, smoothing weight λ, detail scale σ, parameters $\beta_0, \beta_{\max}$
2 **Initialization**: $S^0 \leftarrow I, \beta \leftarrow \beta_0, i \leftarrow 0$
3 **repeat**
4 Calculate $\Re_d(p)$ for each pixel p in $S^{(i)}$
5 Solve for δ_p and ρ_p in Eq. (18)
6 With δ_p and ρ_p, solve for η_p and γ_p in Eq. (26)
7 Minimization for $S^{(i+1)}$ according to η_p and γ_p
8 $\beta \leftarrow 2\beta$, $\sigma \leftarrow \sigma * 0.92$, i ++
9 **until** $\beta > \beta_{\max}$
10 **Output**: image S

3 Experiment and analysis

3.1 Discussion of parameters

There are 3 significant parameters: α, σ and λ in the proposed method. α is a parameter which enhances the discrimination between structure and texture, σ determines the spatial scale of the texture features, and λ is the parameter controlling the smoothness of the image.

3.1.1 Discussion of parameter α

Fig. 3 shows the results with different α values (for $\sigma = 3$, $\lambda = 0.8$). With the increase of α, the discrimination between texture and edge structures becomes larger. In the close-up images, it can be seen that some low-contrast image structures can be better preserved. But the performance of the method on texture smoothing becomes worse with bigger α. Therefore, the parameter α in the experiments is set to [6, 7] as a compromise.

3.1.2 Discussion of parameter σ

The parameter σ in Eq. (5) controls the spatial weights, also determines the window size for computing the windowed variations. With the decrease of σ (for $\alpha = 6$, $\lambda = 0.8$), the difference of $\mathfrak{R}_d$ between weak edges and textures gets smaller, which destroys the weak edge structures. Fig. 4 shows that the region of skirt hem and feet becomes more blurred as σ decreases. But σ cannot be set too big, which may result in that the texture near the edges cannot be completely removed.

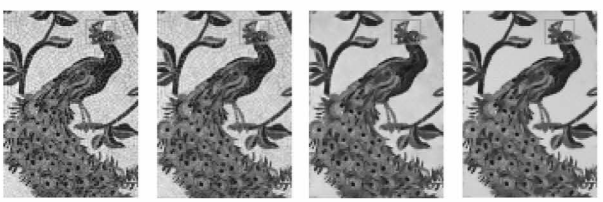

(a) Input (b) S^1 (c) S^3 (d) S^7

Fig. 2 Smoothing results with different iteration

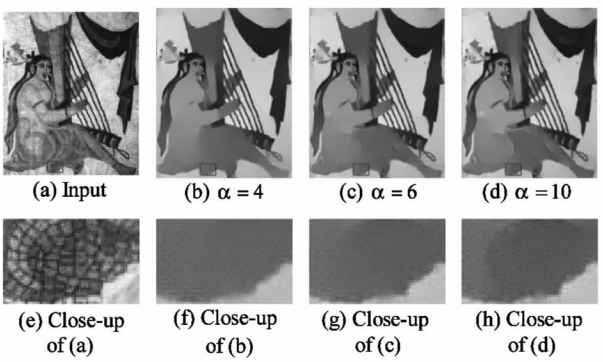

(a) Input (b) $\alpha = 4$ (c) $\alpha = 6$ (d) $\alpha = 10$

(e) Close-up of (a) (f) Close-up of (b) (g) Close-up of (c) (h) Close-up of (d)

Fig. 3 Effect of parameter α

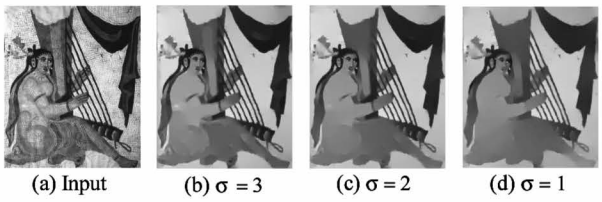

(a) Input (b) $\sigma = 3$ (c) $\sigma = 2$ (d) $\sigma = 1$

Fig. 4 Effect of parameter σ

3.1.3 Discussion of parameter λ

With the increase of λ, the fidelity becomes weaker, and the structure sparsity increases, which promotes the smoothness of the result images. Fig. 5 exhibits that the output image becomes smoother as λ increases (for $\alpha = 6$, $\sigma = 3$). That is, more weak edges and textures are smoothed, and only a few main structures are preserved. But in practice, if λ is too large, the image will be over-smoothing.

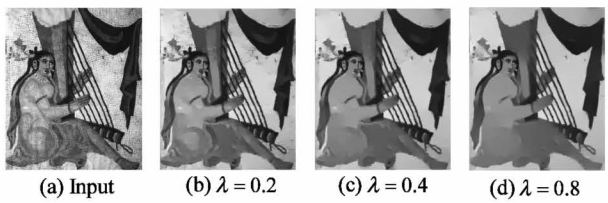

(a) Input (b) $\lambda = 0.2$ (c) $\lambda = 0.4$ (d) $\lambda = 0.8$

Fig. 5 Effect of parameter λ

3.2 Comparison with other methods

As shown in Section 2, the problem of texture smoothing and edge preserving is solved in a new L_0-norm minimization model, the validity of the new objective function and the effectiveness of corresponding approximate solution are demonstrated in Fig. 6 and Fig. 7 by comparing the results with other 3 methods, including L_0 smoothing[12], RTV[17] and mRTV[18].

The test environment is an Acer MS2360 laptop, and the software environment is MatlabR2015b. For the sake of the objectivity and fairness of the experimental results, the parameters of each method are adjusted to the best. The parameters of each method in Fig. 6 are L_0 smoothing $\lambda = 0.08$; RTV $\sigma = 3$, $\lambda = 0.015$; mRTV: $\sigma = 3$, $\lambda = 0.003$; the method $\alpha = 7$, $\sigma = 3$, $\lambda = 1.3$. The parameters of each method in Fig. 7 are: L_0 smoothing $\lambda = 0.08$; RTV $\sigma = 2$, $\lambda = 0.015$; mRTV: $\sigma = 2$, $\lambda = 0.002$; the proposed method $\alpha = 3.2$, $\sigma = 3$, $\lambda = 0.2$.

Since the L_0 smoothing method is heavily dependent on the magnitude of image gradients, it fails to preserve weak edges with small gradients, thus the edges on the middle pumpkin are blurred seriously in Fig. 6(g). After applying RTV and mRTV to distinguish textures and edges of image, the results of the RTV and mRTV are significantly improved. And the proposed method

achieves better results than mRTV by preserving sharper edges on the middle pumpkin in Fig. 6(j).

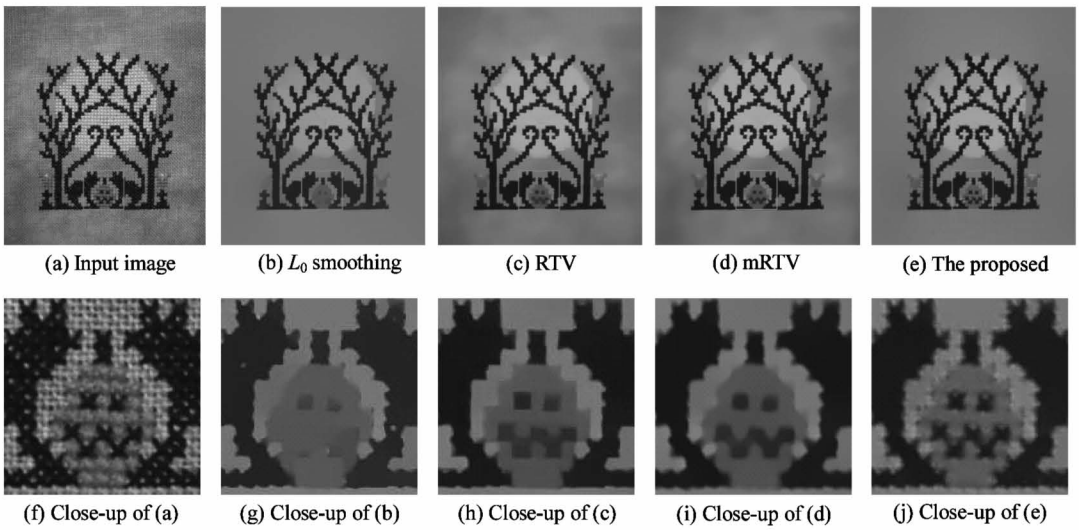

Fig. 6 Smoothing results and comparison on Crossstitch

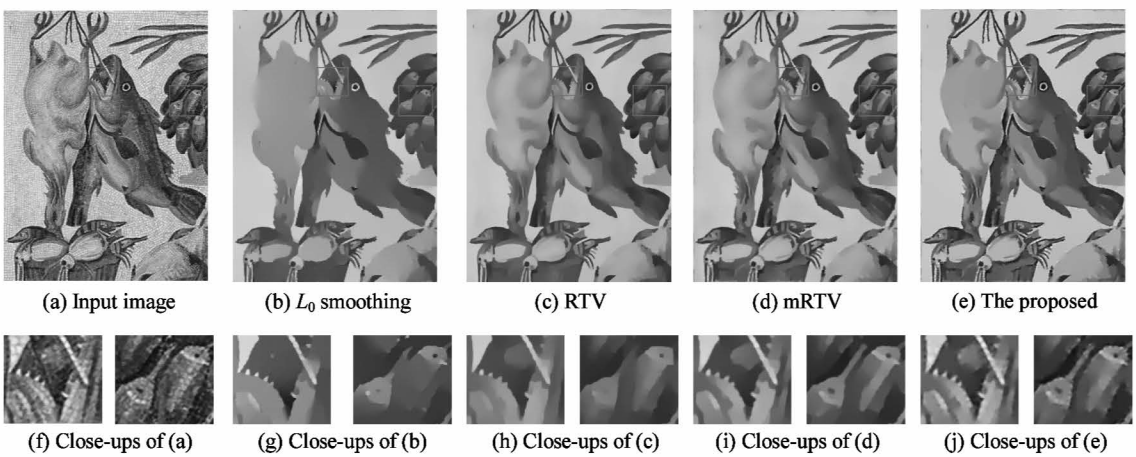

Fig. 7 Smoothing results and comparison on Fish

Compared with Figs7(b), (c) and (d), the proposed method can better preserve the edges with small size or weak gradients and in the image in Fig. 7(e), such as the teeth of fish and the structures on fruits.

For the sake of fairness, the edge peak signal-to-noise ratio (EPSNR) and edge structural similarity index (ESSIM)[20] are used to quantitatively illustrate the smoothing effect of the proposed method. EPSNR/ESSIM is to calculate the PSNR/SSIM value of the input image and the output image after Canny edge detection. The larger the EPSNR/ESSIM value, the better the ability of the method to maintain the structure. As can be seen from Table 2, the EPSNR , ESSIM values of the proposed method in Figs6 and 7 are higher than those of other methods.

Table 2 The EPSNR/ESSIM values with different filters

Filters	Crossstitch (Fig. 6)		Fishmosaic (Fig. 7)	
	EPSNR	ESSIM	EPSNR	ESSIM
L_0	28.9471	0.9807	28.8280	0.9904
RTV	29.1139	0.9806	29.4176	0.9907
mRTV	28.9712	0.9802	29.4991	0.9909
Proposed	29.1761	0.9808	29.9334	0.9913

4 Conclusion

A new objective function is constructed for texture smoothing and edge preserving. The success comes from 2 aspects. First, a novel optimization model is proposed to capture the structures of input images. Second, an efficient approximate solution is given by transforming the original non-linear and non-convex op-

timization problem to a set of subproblems that can be solved iteratively. In the future work, a variety of applications will be explored for totally applying the proposed method, such as detail enhancement, inverse halftone, and edge detection.

References

[1] Xu P P, Wang W C. Improved bilateral texture filtering with edge-aware measurement[J]. *IEEE Transactions on Image Processing*, 2018, 27(7): 3621-3630

[2] Su Z, Luo X N, Deng Z J, et al. Edge-preserving texture suppression filter based on joint filtering schemes[J]. *IEEE Transactions on Multimedia*, 2013, 15(3): 535-548

[3] Fang C W, Liao Z C, Yu Y Z. Piecewise flat embedding for image segmentation[J]. *IEEE Transactions on Pattern Analysis and Machine Intelligence*, 2019, 41(6): 1470-1485

[4] Shital V. Study and analysis of image segmentation techniques for food images[J]. *International Journal of Computer Applications*, 2016, 136(4): 20-24

[5] Teffahi H, Yao H. D-SS frame: deep spectral-spatial feature extraction and fusion for classification of panchromatic and multispectral images[J]. *High Technology Letters*, 2018, 24(4): 378-386

[6] Ren H D, Zhao S M, Gruska J. Edge detection based on single-pixel imaging[J]. *Optics Express*, 2018, 26(5): 5501-5511

[7] Manassi M, Whitney D. Multi-level crowding and the paradox of object recognition in cutter[J]. *Current Biology*, 2018, 28(3): R127-R133

[8] Uijlings J R R, Van De Sande K E A, Gevers T, et al. Selective search for object recognition[J]. *International Journal of Computer Vision*, 2013, 104(2): 154-171

[9] Abeed M A, Biswas A K, Al-Rashid M, et al. Image processing with dipole-coupled nano- magnets: noise suppression and edge enhancement detection[J]. *IEEE Transactions on Electron Devices*, 2017, 64(5): 2417-2424

[10] Talebi H, Milanfar P. Learned perceptual image enhancement[C]// IEEE International Conference on Computational Photography, Pittsburgh Pennsylvania, USA, 2018: 1-13

[11] Kang S B, Kapoor A, Lischinski D. Personalization of image enhancement[C]// IEEE Computer Society Conference on Computer Vision and Pattern Recognition, San Francisco, USA, 2010: 1799-1806

[12] Xu L, Lu C, Xu Y, et al. Image smoothing via L_0 gradient minimization[J]. *ACM Transactions on Graphics*, 2011, 30(6): 1-12

[13] Farbman Z, Fattal R, Lischinski D, et al. Edge-preserving decompositions for multi-scale tone and detail manipulation[J]. *ACM Transactions on Graphics*, 2008, 27(3): 67-76

[14] Tomasi C, Manduchi R. Bilateral filtering for gray and color images[C]// The 6th International Conference on Computer Vision, Bombay, India, 1998: 839-846

[15] Shen C T, Chang F J, Hung Y P, et al. Edge-preserving image decomposition using L_1 fidelity with L_0 gradient[C]// Special Interest Group for Computer Asia 2012 Technical Briefs, New York, USA, 2012: 1-4

[16] Cheng X, Zeng M, Liu X. Feature-preserving filtering with L_0 gradient minimization[J]. *Computers and Graphics*, 2014, 38(1): 150-157

[17] Xu L, Yan Q, Xia Y, et al. Structure extraction from texture via relative total variation[J]. *ACM Transactions on Graphics*, 2012, 31(6): 139-148

[18] Sun Y J, Schaefer S, Wang W P. Image structure retrieval via L_0 minimization[J]. *IEEE Transaction on Visualization and Computer Graphics*, 2018, 24(7): 2129-2139

[19] Liu Q G, Xiong B, Yang D C, et al. A generalized relative total variation method for image smoothing[J]. *Multimedia Tools and Applications*, 2016, 75(13): 7909-7930

[20] Zhao L J, Bai H H, Wang A H, et al. Iterative range domain weighted filter for structural preserving image smoothing and de-noising[J]. *Multimedia Tools and Applications*, 2019, 78(1): 47-74

Nie Dongdong, born in 1977. She received her Ph. D degree from Shanghai Jiao Tong University in 2007. She is an associate professor in the College of Sciences, Yanshan University. Her research interests include image processing, pattern recognition and computer vision.